NANO EXPRESS

Open Access

Facile method to synthesize magnetic iron oxides/TiO$_2$ hybrid nanoparticles and their photodegradation application of methylene blue

Wei Wu[1,2,3], Xiangheng Xiao[1,2], Shaofeng Zhang[1,2], Feng Ren[1,2] and Changzhong Jiang[1,2*]

Abstract

Many methods have been reported to improving the photocatalytic efficiency of organic pollutant and their reliable applications. In this work, we propose a facile pathway to prepare three different types of magnetic iron oxides/TiO$_2$ hybrid nanoparticles (NPs) by seed-mediated method. The hybrid NPs are composed of spindle, hollow, and ultrafine iron oxide NPs as seeds and 3-aminopropyltriethyloxysilane as linker between the magnetic cores and TiO$_2$ layers, respectively. The composite structure and the presence of the iron oxide and titania phase have been confirmed by transmission electron microscopy, X-ray diffraction, and X-ray photoelectron spectra. The hybrid NPs show good magnetic response, which can get together under an external applied magnetic field and hence they should become promising magnetic recovery catalysts (MRCs). Photocatalytic ability examination of the magnetic hybrid NPs was carried out in methylene blue (MB) solutions illuminated under Hg light in a photochemical reactor. About 50% to 60% of MB was decomposed in 90 min in the presence of magnetic hybrid NPs. The synthesized magnetic hybrid NPs display high photocatalytic efficiency and will find recoverable potential applications in cleaning polluted water with the help of magnetic separation.

Keywords: magnetic iron oxide nanoparticles, TiO$_2$, hybrid structure, photocatalyst, methylene blue

Introduction

Extended and oriented nanostructures are desirable for many applications, but facile fabrication of complex nanostructures with controlled crystalline morphology, orientation, and surface architectures remains a significant challenge [1]. Among their various nanostructured materials, magnetic NPs-based hybrid nanomaterials have attracted growing interests due to their unique magnetic properties. These functional composite NPs have been widely used in various fields, such as magnetic fluids, data storage, catalysis, target drug delivery, magnetic resonance imaging contrast agents, hyperthermia, magnetic separation of biomolecules, biosensor, and especially the isolation and recycling of expensive catalysts [2-12]. To this end, magnetic iron oxide NPs became the strong candidates, and the application of small iron oxide NPs has been practiced for nearly semicentury owing to its simple preparation methods and low cost approaches [13].

Currently, semiconductor NPs have been extensively used as photocatalyst. TiO$_2$ NPs have been used as aphotocatalytic purification of polluted air or wastewater, will become a promising environmental remediation technology because of their high surface area, low cost, nontoxicity, high chemical stability, and excellent degradation for organic pollutants [14-17]. Moreover, TiO$_2$ also bears tremendous hope in helping to ease the energy crisis through effective utilization of solar energy based on photovoltaic and water-splitting devices [18-21]. As comparing with heterogeneous catalysts, many homogenerous catalytic systems have not been commericalized because of one major disadvantage: the difficulty of separation the reaction product from the catalyst and from any reaction solvent for a long and sustained environment protection [22]. In addition, there are two bottleneck drawbacks associated with TiO$_2$ photocatalysis currently, namely, high charge recombination rate inherently and low efficiency for

* Correspondence: czjiang@whu.edu.cn
[1]Key Laboratory of Artificial Micro- and Nano-structures of Ministry of Education, Wuhan University, Wuhan 430072, People's Republic of China
Full list of author information is available at the end of the article

Springer

utilizing solar light, which would greatly hinder the commercialization of this technology [23]. Currently, the common methods are metals/non-metals-doping or its oxides-doping to increasing the utilization of visible light and enhancing the separation situation of charge carriers [24-27]. More importantly, the abuse and over-use of photocatalyst will also pollute the enviroment.

In this point, magnetic separation provides a convenient method to removing pollutants and recycling magnetized species by applying an appropriate external magnetic field. Therefore, immobilization of TiO_2 on magnetic iron oxide NPs has been investigated intensely due to its magnetic separation properties [28-32]. Indeed, the study of core-shell magnetic NPs has a wide range of applications because of the unique combination of the nanoscale magnetic iron oxide core and the functional titania shell. Although some publications reported the synthesis of iron oxide-TiO_2 core-shell nanostructure, these reported synthesis generally employed solid thick SiO_2 interlayer. For instance, Chen et al. reported using TiO_2-coated Fe_3O_4 (with a silica layer) core-shell structure NPs as affinity probes for the analysis of phosphopeptides and as a photokilling agent for pathogenic bacteria [33,34]. Recently, Wang et al. reported the synthesis of $(\gamma\text{-}Fe_2O_3@SiO_2)_n@TiO_2$ functional hybrid NPs with high photocatalytic efficiency [35]. Generally, immobilization of homogeneous catalysts usually decreases the catalytic activity due to the problem of diffusion of reactants to the surface-anchored catalysts [36]. In order to increase the active surface area, hollow and ultrafine iron oxide NPs are employed in this paper. Moreover, we proposed a new utilization of magnetic NPs as a catalyst support by modifying the surface on three different-shaped amino-functionalized iron oxide NPs with an active TiO_2 photocatalytic layer via a seed-mediate method, as shown in Figure 1. The surface amines on the magnetic iron oxide NPs can serve as functional groups for further modification of titania. We discuss the formation mechanism of iron oxide/TiO_2 hybrid NPs. The results maybe provide some new insights into the growth mechanism of iron oxide-TiO_2 composite NPs. It is shown that the as-synthesized iron oxide/TiO_2 hybrid NPs display good magnetic response and photocatalytic activity. The magnetic NPs can be used as a MRCs vehicle for simply and easily recycled separation by external magnetic field application.

Experiment
Reagents and materials
$FeCl_3 \cdot 6H_2O$, $FeCl_2 \cdot 4H_2O$, $FeSO_4 \cdot 7H_2O$, and KOH were purchased from Tianjin Kermel Chemical Reagent Co., Ltd. (Tianjin, China); KNO_3, L(+)-glutamic acid (Gla, $C_5H_9NO_4$), tetrabutyl titanate (Ti(Bu)$_4$, Bu = OC_4H_9, CP) and methylene blue were purchased from

Sinopharm Chemical Reagent CO., Ltd. (Shanghai, China); cetyltrimethylammmonium bromide (CTAB, $C_{19}H_{42}BrN$, ultrapure), MB and hexamethylenetetramine ($C_6H_{12}N_4$) were purchased from Aladdin Chemical Reagent CO., Ltd. (Shanghai, China); 3-aminopropyl-triethyloxysilane (APTES) were purchased from Sigma (St. Louis, MO, USA), and all the reagents are analytical pure and used as received.

Preparation of iron oxide seeds
A. Spindle hematite NPs
According to Ishikava's report [37], we take a modified method to prepare the monodisperse spindle hematite NPs, in a typical synthesis, 1.8 ml of a 3.7 M $FeCl_3 \cdot 6H_2O$ solution was added dropwise into 4.5×10^{-4} M NaH_2PO_4 solution at 95°C and the mixture was aged at 100°C for 12 h. The resulting precipitates were washed with a 1 M ammonia solution and doubly distilled water and finally dried under vacuum.

B. Hollow magnetite NPs
According to our previous report [38], in a typical synthesis, solution A was prepared by dissolving 2.02 g KNO_3 and 0.28 g KOH in 50 mL double distilled water, solution B was prepared by dissolving 0.070 g $FeSO_4 \cdot 7H_2O$ in 50 mL double distilled water. Then the two solution were mixed together under magnetic stirring at a rate of ca. 400 rpm. Two minutes later, solution C (0.18 g Gla in 25 mL double distilled water) was added dropwise into the mixed solution. The reaction temperature was raised increasingly to 90°C and kept 3 h under argon (Ar) atmosphere. Meanwhile, the brown solution was observed to change black. After the mixture was cooled to room temperature, the precipitate products were magnetically separated by MSS, washed with ethanol and water two times, respectively, and then redispersed in ethanol.

C. Ultrafine magnetite NPs
The ultrafine magnetite NPs were prepared through the chemical co-precipitation of Fe(II) and Fe(III) chlorides (Fe^{II}/Fe^{III} ratio = 0.5) with 0.5 M NaOH [39]. The black precipitate was collected on a magnet, followed by rinsing with water several times until the pH reached 6 to 7.

Preparation of amino-functionalized iron oxide NPs
A solution of APTES was added into the above seed suspensions, stirred under Ar atmosphere at 25°C for 4 h. The prepared APTES-modified seeds were collected with a magnet, and washed with 50 mL of ethanol, followed by double distilled water for three times [40].

Preparation of iron oxides/TiO_2 hybrid NPs
In a typical synthesis, 0.2 g amino-functionalized seeds, 0.2 g CTAB, and 0.056 g HMTA were dissolved in 25 ml ethanol solution under ultrasonic condition at room
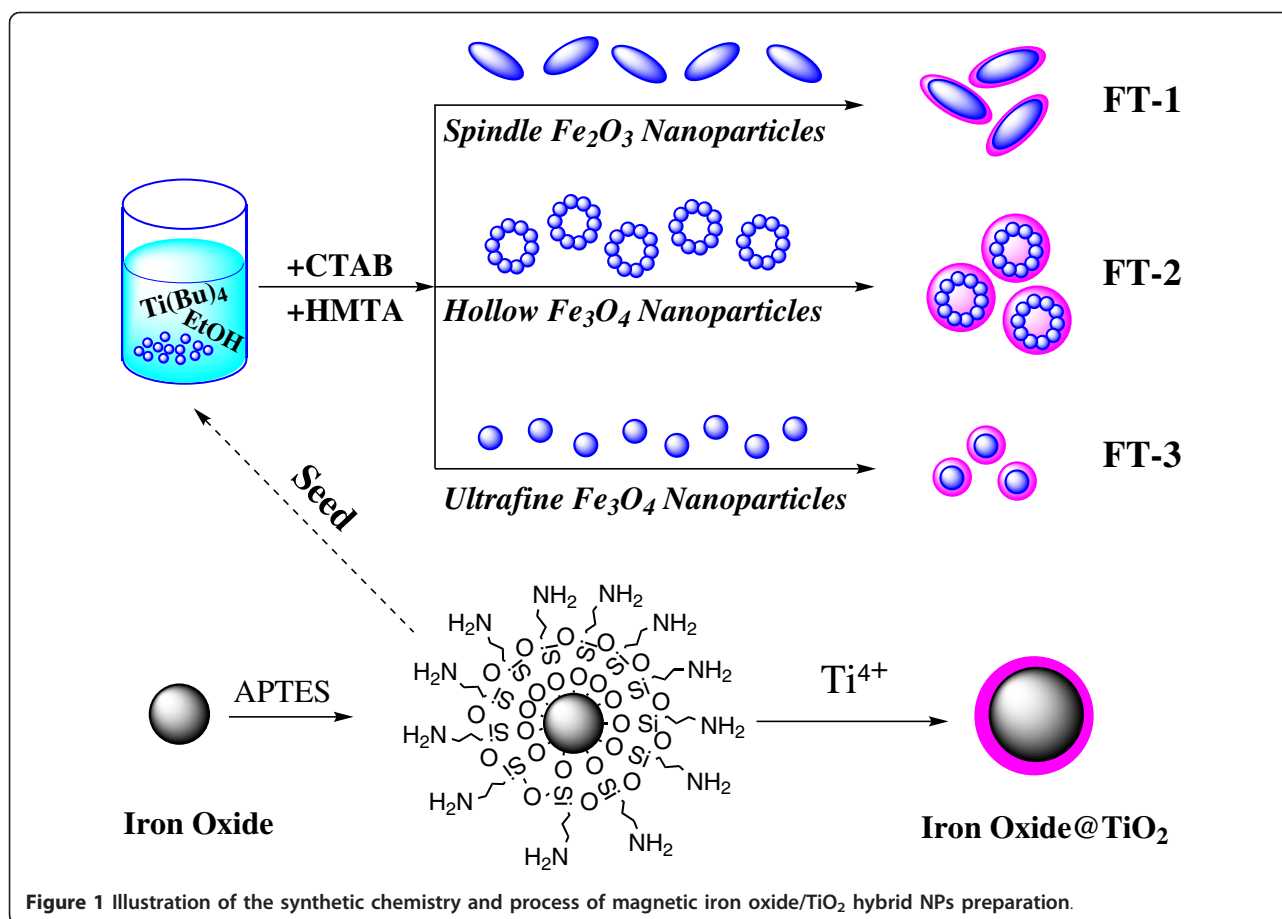
Figure 1 Illustration of the synthetic chemistry and process of magnetic iron oxide/TiO$_2$ hybrid NPs preparation.

temperature. The mixture solution was then transferred into a Teflon-lined tube reactor. Then, 1 ml Ti(Bu)$_4$ dropwise added in the tube, and was kept at 150°C for 8 h.

Photodegradation of MB

The prepared samples were weighed and added into 80 mL of methylene blue solutions (12 mg/L). The mixed solutions were illuminated under mercury lamp (OSRAM, 250 W with characteristic wavelength at 365 nm), and the MB solutions were illuminated under UV light in the photochemical reactor. The solutions were fetched at 10-min intervals by pipette for each solution and centrifuged. Then, the time-dependent absorbance changes of the transparent solution after centrifugation were measured at the wavelength between 500 and 750 nm.

Characterization

TEM images were performed with a JEOL JEM-2010 (HT) (JEOL, Tokyo, Japan) transmission electron microscope operating at 200 kV, and the samples were dissolved in ethanol and dropped on super-thin cabon coated copper grids. SEM studies were carried out using a FEI Sirion FEG operating at 25 keV, samples were sprinkled onto the conductive substrate, respectively. Powder X-ray diffraction (XRD) patterns of the samples were recorded on a D8 Advance X-ray diffractometer (Germany) using Cu Kα radiation (λ = 0.1542 nm) operating at 40 kV and 40 mA and with a scan rate of 0.05° 2θ s^{-1}. X-ray photoelectron spectroscopy (XPS) measurements were made using a VG Multilab2000X. This system uses a focused Al exciting source for excitation and a spherical section analyzer. The percentages of individual elements detection were determined from the relative composition analysis of the peak areas of the bands. Magnetic measurements were performed using a Quantum Design MPMS XL-7 SQUID magnetometer. The powder sample was filled in a diamagnetic plastic capsule, and then the packed sample was put in a diamagnetic plastic straw and impacted into a minimal volume for magnetic measurements. Background magnetic measurements were checked for the packing material. The diffuse reflectance, absorbance and transmittance spectra, and photodegradation examination of the microspheres was carried out in a PGeneral TU-1901 spectrophotometer.
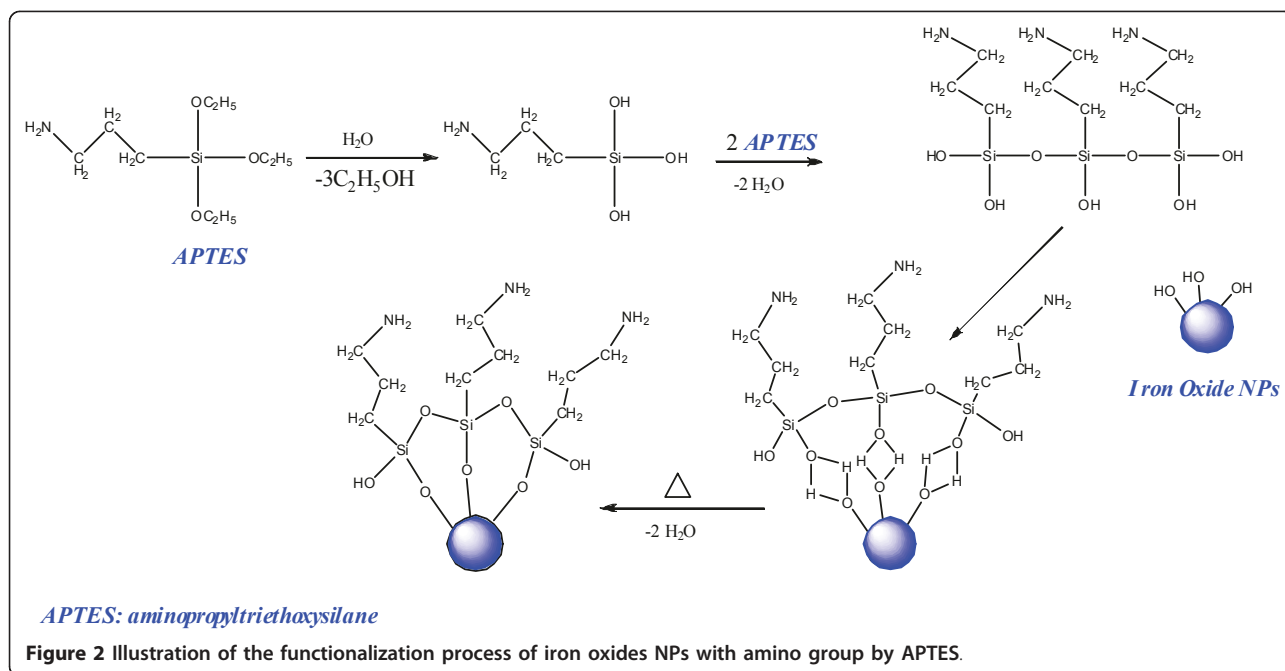
Results and discussion

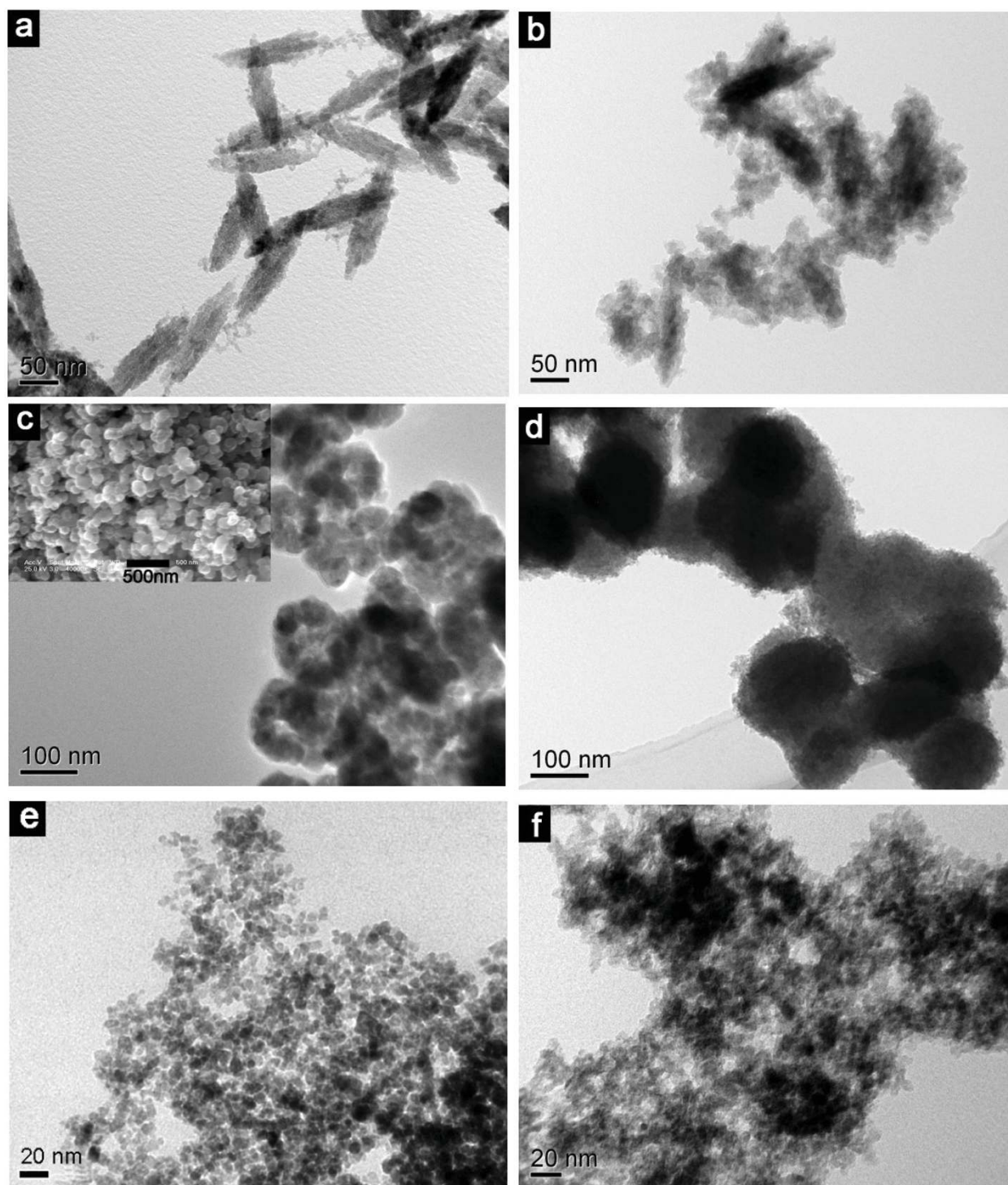### Formation mechanism and morphology

For the synthesis of the functional hybrid nanomaterials, we synthesized the colloidal solutions of iron oxides NPs with different shapes in ethanol at the first. These iron oxide NPs exhibit long sedimentation time, and are stable against agglomeration for several days. Then, iron oxides NPs were modified with amino group by APTES because silane can render highly stability and water-dispersibility, and it also forms a protective layer against mild acid and alkaline environment. As shown in Figure 2, hydroxyl groups (-OH) on the magnetite surface reacted with the -OH of the APTES molecules leading to the formation of Si-O bonds and leaving the terminal -NH_2 groups available for immobilization of TiO_2 [41]. The immobilization of TiO_2 can be explained by HSAB (hard and soft acids and bases) formula [42]. As a typical hard acid, Ti ions can be combined to the terminal -NH_2 groups (hard bases) easily, owing to there is small amount water in ethanol (95%), and then TiO_2 will be coated on the surface of amino-functionalized iron oxide NPs by hydrolysis and poly-condensation as follows:

$$\text{(1)}$$

$$\text{(2)}$$

We prepared the monodisperse spindle-like iron oxide NPs by ferric hydroxide precipitate method for evaluating and verifying our experimental mechanism and functional strategies. The electron micrograph of

the starting weak-magnetic spindle-like hematite NPs are shown in Figure 3a, which have longitudinal diameter in the range from 120 to 150 nm and transverse diameter (short axis) around 40 nm. After TiO_2 coating (FT-1), the transverse diameter increased to around 50 nm, and the representative image is shown in Figure 3b. Moreover, the obvious contrast differences between the pale edges and dark centers further clearly confirms the composite structure. Therefore, the results reveal that this functional strategy for fabricating the TiO_2-functionalized iron oxide NPs is a feasible approach. Then, two strong magnetic iron oxide NPs with different shape and diameter as seeds were employed to fabricate the magnetic TiO_2 hybrid materials. As shown in Figure 3c, Fe_3O_4 NPs with an obviously hollow structure have diameters around 100 nm, and the insert field-emission SEM image illustrates the hollow NPs present sphere-like shape. In our previous report, we have confirmed that the hollow Fe_3O_4 NPs were formed by oriented aggregation of small Fe_3O_4 NPs [38]. Figure 3d shows bright field TEM image of the corresponding iron oxide NPs after the same TiO_2 coating process (FT-2). However, the hybrid NPs present a shagginess sphere-like shape and cannot observe the hollow structure. Additionally, the diameters of hybrid NPs increased about 5 to 10 nm. The results reveal that the hollow Fe_3O_4 NPs have been covered by TiO_2. Owing to the loose struture of Fe_3O_4 seeds, TiO_2 will fill to its internal and surface, and finally cause the hybrid products present a solid nature. The diameter of above two different iron oxide

Figure 2 Illustration of the functionalization process of iron oxides NPs with amino group by APTES.

Figure 3 Representative TEM images of naked iron oxides and iron oxides/TiO$_2$ hybrid NPs. The insert in **(c)** is the corresponding SEM image.

NPs including spindle-like and hollow is relatively large, subsequently, we employ the ultrafine Fe$_3$O$_4$ NPs as seeds to fabricate the hybrid NPs. Figure 3e presents the TEM images of ultrafine Fe$_3$O$_4$ NPs without any size selection, the size is about 5 to 8 nm. By introduce the TiO$_2$, the as-obtained products (FT-3) exhibit an aggregated nature and the ultrafine Fe$_3$O$_4$ NPs dispersing in the TiO$_2$ matrix, as shown in Figure 3f.

Structure and composition

XRD and XPS surface analysis was used to further confirm the structure and composition of iron oxides/TiO_2 hybrid NPs. Figure 4a shows the XRD patterns of the as-synthesized α-Fe_2O_3 seeds and α-Fe_2O_3/TiO_2 (FT-1). From the XRD patterns of α-Fe_2O_3 seeds, it can be seen that the diffraction peaks conformity with that of rhombohedral α-Fe_2O_3 (JCPDS no. 33-0664, show in the
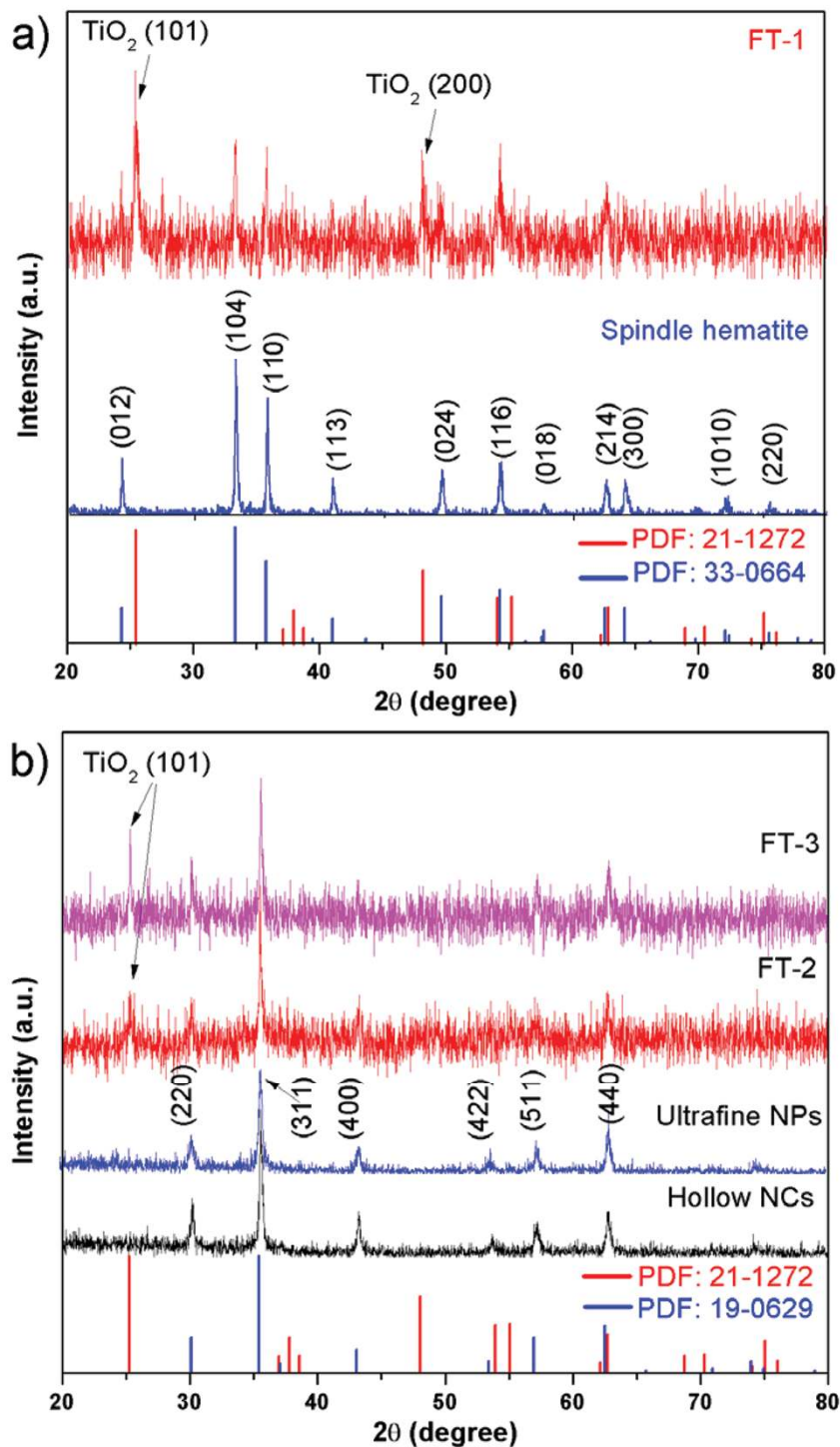
Figure 4 XRD patterns. Patterns of the as-prepared spindle-like α-Fe_2O_3 NPs and FT-1 **(a)**, as-prepared hollow and ultrafine Fe_3O_4 NPs, FT-2 and FT-3 **(b)**.

bottom). After coating, compared with that data of JCPDS no. 33-0664 and JCPDS no. 21-1272 (pure anatase TiO_2 phase), the (101) and (200) peaks of anatase TiO_2 can be found in FT-1, suggesting that α-Fe_2O_3/TiO_2 composite NPs are successfully fabricated by this method. Figure 4b shows the XRD patterns of the as-synthesized Fe_3O_4 seeds and Fe_3O_4/TiO_2 (FT-2 and FT-3). All peaks in the XRD patterns of both seeds can be perfectly indexed to the cubic Fe_3O_4 structure (JCPDS no. 19-0629, show in the bottom). After coating, the (101) peak of anatase TiO_2 can be clearly found in FT-2 and FT-3, suggesting that Fe_3O_4/TiO_2 hybrid NPs are successfully synthesized.

Figure 5 is the typical XPS spectra of the naked, amino-functionalized, and titania coating ultrafine Fe_3O_4 NPs, where part (a) is the survey spectrum and parts (b) to (d) are the high-resolution binding energy spectrum for Fe, Si, O, and Ti species, respectively. According to the survey spectrum, the elements of Fe, O, and C are found in the naked ultrafine Fe_3O_4 NPs, of which the element of C is found on the surface as the internal reference, and the elements of Fe and O arise from the components of Fe_3O_4. The new signals of N 1s, Si 2s, and Si 2p are observed in APTES-coated Fe_3O_4 NPs, and the new signal of Ti 2p signals is observed in FT-3 hybrid NPs. These results indicate that the FT-3 are composed of two components, silane functionalized Fe_3O_4 and TiO_2. It is noteworthy that many studies demonstrated that if particles possessed a real core and shell structure, the core would be screened by the shell and the compositions in the shell layer became gradually more dominant, the intensity ratio of the shell/core spectra would gradually increase [43-47]. The gradually subdued XPS signals of Fe after TiO_2 coating are discerned in Figure 5b. APTES coating increases the intensity of carbon and oxygen, and decreases the concentration of Fe; further TiO_2 coating decreases the intensity of silicon and Fe (as shown in Figure 5b, c). Therefore, after TiO_2 coating, corresponding XPS signals of Fe, and Si rule also are decreased, C and O do not match with this rule due to the formation of TiO_2 and surfactant impurities (as shown in Figure 5d, e). Additionally, interactions should exist among APTES-coated Fe_3O_4 NPs and titania which cause the shift of binding energy of Fe. Usually, XPS measures the elemental composition of the substance surface up to 1 to 10 nm depth. Therefore, XPS could be regarded as a bulk technique due to the ultrafine particles size of the FT-3 (less than 10 nm). The XPS result indicates that the amino-functionalized Fe_3O_4 seeds have been coated by a TiO_2 layer, thus greatly reducing the intensity signals of the element inside. Table 1 lists the binding energy values of Fe, Si, O, N, and Ti resolved from XPS spectra of the above three different NPs. In three cases,

the value of binding energy of Fe 2p and other elements are very close to the standard binding energy values. Relative to the standard values [48], the binding energy values in FT-3 have decreased and this result is in agreement with the previous discussions.

Furthermore, XPS surface analysis is also used to quantify the amount of titanium and iron present in the near surface region of the three different hybrid NPs. Figure 6 is the typical XPS spectra of the FT-1, FT-2, and FT-3, where part (a) is the survey spectrum and parts (b)-(d) are the high-resolution binding energy spectrum for Fe, Si, O, C, N, and Ti species, respectively. According to the survey spectrum, all hybrid NPs exhibited typical binding energies at the characteristic peaks of Ti 2p, Fe 2p, Si 2p, N 1s and O1s in the region of 458, 710, 103, 400, and 530 eV, respectively. Details of the XPS surface elemental composition results of as-obtained products are shown in Table 2. The XPS data of the titanium-to-iron ratio of hybrid NPs is calculated in which the elemental composition ratio of FT-1, FT-2, and FT-3 (titanium/iron) are about 2:1, 3.5:1, and 5.5:1. The results reveal that the quantity of Ti element is higher than that of Fe element on the surface of samples. That is, it may deduce that iron oxide NPs have been coated by TiO_2. In all hybrid NPs, the amount of oxygen to titanium or iron calculated from XPS data is about 5:1, this results is in agreement with the other reports [49]. Nevertheless, the combined results from TEM and XPS suggest that the synthesized hybrid NPs are composed of amino-functionalized iron oxide NPs and TiO_2.

Magnetic and magnetic response properties

Magnetic measurements of the hybrid NPs were performed on a SQUID magnetometer. As shown in Figure 7, hysteresis loops demonstrate that FT-2 and FT-3 have no hysteresis, the forward and backward magnetization curves overlap completely and are almost negligible. Moreover, the NPs have zero magnetization at zero applied field, indicating that they are superparamagnetic at room temperature, no remnant magnetism was observed when the magnetic field was removed [50]. Superparamagnetism occurs when the size of the crystals is smaller than the ferromagnetic domain (the size of iron oxide NPs should less than 30 nm), the size of the ultrafine Fe_3O_4 component in our product is less than 10 nm, and the hollow Fe_3O_4 is consist of small magnetite NPs, there are reasonable to suppose that the hybrid NPs showed superparamagnetic behavior. The results reveal that the products have been inherit the superparamagnetic property from the Fe_3O_4 NPs, and the saturation magnetization value (M_s) of naked hollow Fe_3O_4 and ultrafine Fe_3O_4 is 89.2 and 72.1 emu/g, respectively. After TiO_2 coating, the corresponding
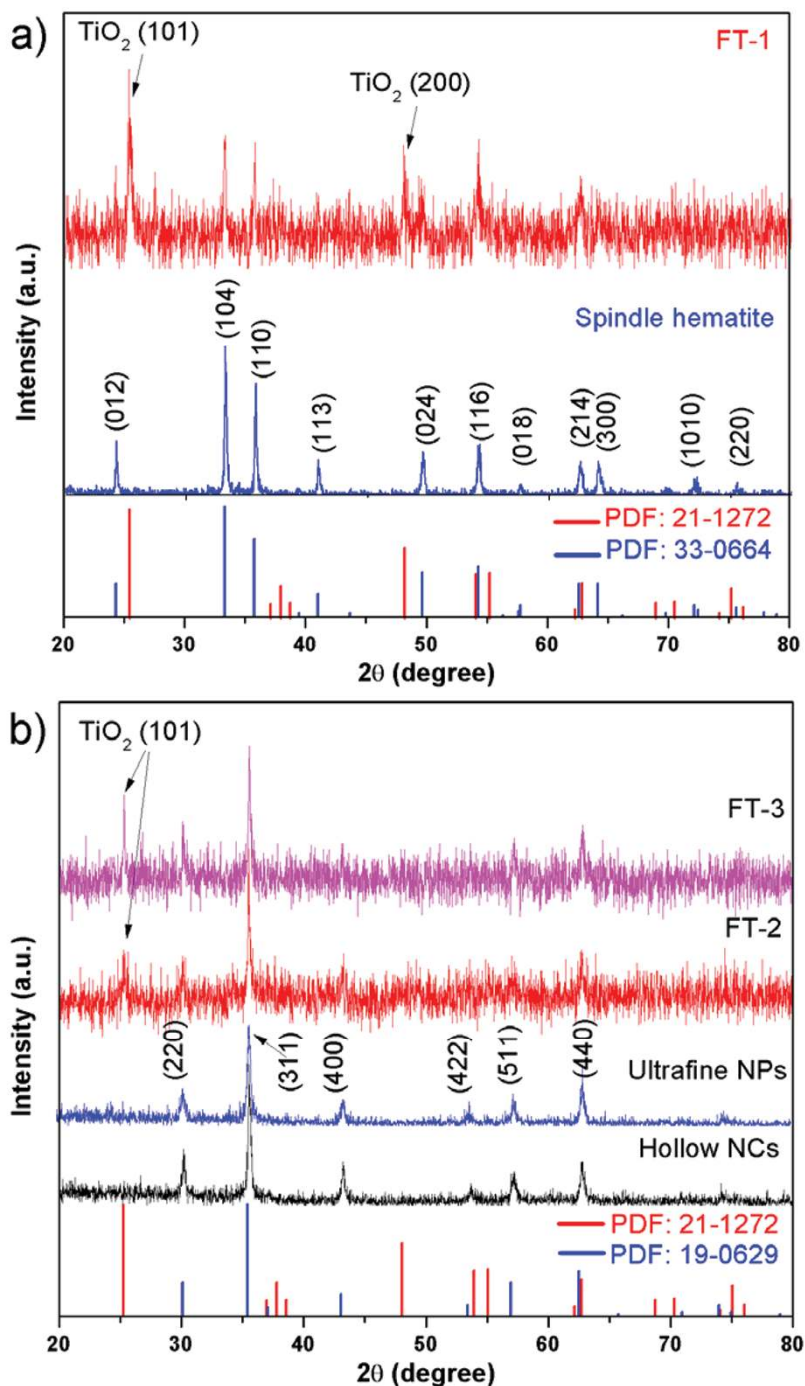
Figure 5 XPS spectra of the naked, amino-functionalized, and titania coating ultrafine Fe₃O₄ NPs. XPS spectra for ultrafine Fe$_3$O$_4$ NPs (curve a), APTES-coated ultrafine Fe$_3$O$_4$ NPs (curve b) and ultrafine Fe$_3$O$_4$/TiO$_2$ hybrid NPs (curve c) comparison **(a)**, the regions for Fe 2*p* **(b)**, Si 2*p* **(c)**, O 1*s* **(d)**, and C 1*s* **(e)**, comparison respectively.

value of M_s decreases to 16.2 and 5.0 emu/g, respectively. The M_s decreased significantly after coating with TiO$_2$ due to the surface effect arising from the non-collinearity of magnetic moments, which may be due to the coated TiO$_2$ is impregnated at the interface of iron oxide matrix and pinning of the surface spins [51]. Moreover, this decrease in magnetic behavior is very close to other reports [52,53]. As the most stable iron oxide NPs in the ambient conditions, the magnetic properties of hematite are not well understood [54-56].

Table 1 Standard binding energy values

Samples[a]	Fe 2p$_{3/2}$	O 1s	Si 2p	N 1s	Ti 2p$_{3/2}$
Naked Fe$_3$O$_4$ nanoparticles	710.9	531.5			
APTES-coated Fe$_3$O$_4$ nanoparticles	710.5	531.5	102.5	399.5	
Hybrid nanoparticles (FT-3)	710.0	530.0	101.4	400.7	458.3
Standard value	710.5[b]	531.4[c], 529.9[d]	103.3[e]	399.8[f]	458.8[g]

Standard binding energy values for Fe 2p, Si 2p, N 1s, O 1s, and Ti 2p and those resolved in the naked, amino-functionalized, and titania coating ultrafine Fe$_3$O$_4$ nanoparticles. [a]Unit for binding energy: eV; [b]Fe in Fe$_3$O$_4$; [c]O in Fe$_3$O$_4$; [d]O in TiO$_2$; [e]Si in SiO$_2$; [f]N in N-C group; [g] Ti in TiO$_2$, Δ = 5.54 eV

We checked the magnetic properties of FT-1 hybrid NPs, the M_s is about 2×10^{-4} emu/g, and the composite NPs exhibit a typical ferromagnetism. Thereby, as a weak magnetic hybrid NPs, FT-1 cannot be separate by common magnet.

We checked the magnetic responsibility of FT-2 and FT-3 hybrid NPs under the external applied magnetic field by a common magnet. As shown in Figure 8, both hybrid NPs gather quickly without residues left in the solid and solution state when the magnet presence. The gathered hybrid NPs can be redispersed in the solution easily by a slight shake. The results illustrate that the hybrid NPs display a good magnetic response, and this is also important for the industrial application in water cleaning as MRCs for preventing loss of materials and save cost.

Optical adsorption and photocatalytic properties

The three different hybrid NPs were further characterized by UV-vis absorption spectra to compare their optical adsorption properties and the results are shown in Figure 9a. The spectra highlight a strong adsorption in the UV region, the results are in agreement with the other reports [57,58]. It is noteworthy that the hybrid NPs with different morphology (at same concentration) will cause the difference of adsorption intensity and peak location. Due to the small dimensions of semiconductor NPs, a discretization of the bandgap occurs with decreasing particle size, leading to smaller excitation frequencies. A blue shift of FT-3 is observed in the extinction behavior, and the absorption edge is positioned at smaller wavelengths [59]. The result confirms that the diameter of FT-1 hybrid NPs is large than the other two different types hybrid NPs. Additionally, a concomitant tail can be clearly observed in the visible region of the absorption curve owing to scattering losses induced by the large number of inorganic NPs in the composite nanostructure [60].
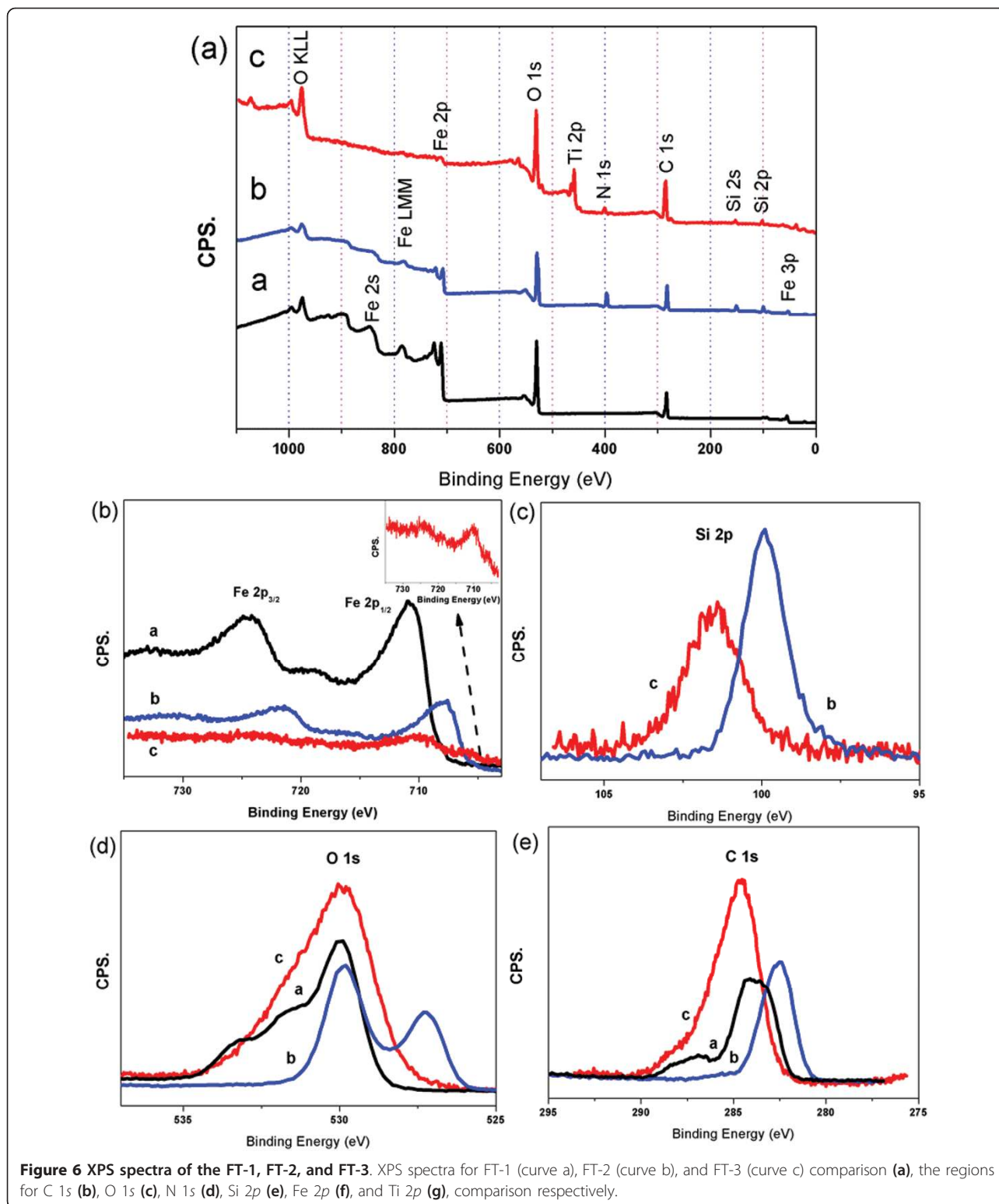
In order to calculate the bandgap of hybrid NPs, the relationship between the absorption coefficient (α) and

the photon energy (hv) have been given by equation as follows: $\alpha hv = A(hv\text{-}E_E)^m$, where A is a constant, E_g is the bandgap energy, hv is the incident photon energy and the exponent m depends on the nature of optical transition. The value of m is 1/2 for direct allowed, 2 for indirect allowed, 3/2 for direct forbidden, and 3 for indirect forbidden transitions [61]. The main mechanism of light absorption in pure semiconductors is direct interband electron transitions. The absorption coefficient α has been calculated from the Lamberts formula [62], $\alpha = \dfrac{1}{t} \ln\left(\dfrac{1}{T}\right)$, where T and t are the transmittance (can be directly measured by UV-vis spectra) and path length of the colloids solution (same concentration), respectively. A typical plot of $(\alpha hv)^2$ versus photon energy (hv) for the samples are shown in Figure 9b. The value of FT-1, FT-2, and FT-3 is 2.85, 2.89, and 2.73 eV, respectively. TiO$_2$ is important for its application in energy transport, storage, and for the environmental cleanup due to its well known photocatalytic effect with a bandgap of 3.2 eV [63]. Comparing with the pure TiO$_2$ NPs, the bandgap of hybrid NPs is obviously decreased, and the absorption edge generates obvious red shift. This red shift is attributed to the charge-transfer transition between the electrons of the iron oxide NPs and the conduction band (or valence band) of TiO$_2$ [64]. Iron oxide NPs can increase energy spacing of the conduction band in TiO$_2$ and finally lead to the quantization of energy levels and causes the absorption in the visible region. The other is that amino groups can act as a substitutional dopant for the place of titanium and change metal coordination of TiO$_2$ and the electronic environment around them [65]. Similar phenomenon of red shift in the bandgap for iron oxide/TiO$_2$ hybrid NPs were also found by other reports [53,65-67].

The photocatalytic activity was examined by a colorant decomposition test using MB, which is very stable chemical dye under normal conditions. In general, absorption spectra can be used to measure the concentration changes of MB in extremely dilute aqueous solution. The MB displays an absorption peak at the wavelength of about 664 nm. Time-dependent photodegradation of MB is shown in Figure 10. It is illustrated that MB decomposes in the presence of magnetic TiO$_2$ hybrid materials. Generally, the pure TiO$_2$ NPs can decompose 40% MB in 90 min [68-70]. In our previous report, the pure TiO$_2$ NPs with a average diameter of 5 nm can be decomposed 53% MB in 90 min [71]. However, in our system, 49.0%, 56.5%, and 49.6% MB decomposed by FT-1, FT-2, and FT-3 in 90 min, respectively. The result reveals that the introduction of iron oxide NPs not only improve the photocatalytic activity but also employ the corresponding magnetic properties from itself. Thus, the

Figure 6 XPS spectra of the FT-1, FT-2, and FT-3. XPS spectra for FT-1 (curve a), FT-2 (curve b), and FT-3 (curve c) comparison **(a)**, the regions for C 1*s* **(b)**, O 1*s* **(c)**, N 1*s* **(d)**, Si 2*p* **(e)**, Fe 2*p* **(f)**, and Ti 2*p* **(g)**, comparison respectively.

as-synthesized magnetic hybrid NPs with high photocatalytic efficiency are very potentially useful for cleaning polluted water with the help of magnetic separation. The photocatalytic degradation generally follows a Langmuir-Hinshelwood mechanism, which could be simplified as a pseudo-first order reaction as follows [72,73]: $r = -\dfrac{dC_t}{dt} = kCt$, where r is the degradation rate

**Table 2 Surface elemental composition and XPS binding energies of FT-1, FT-2, and FT-3**

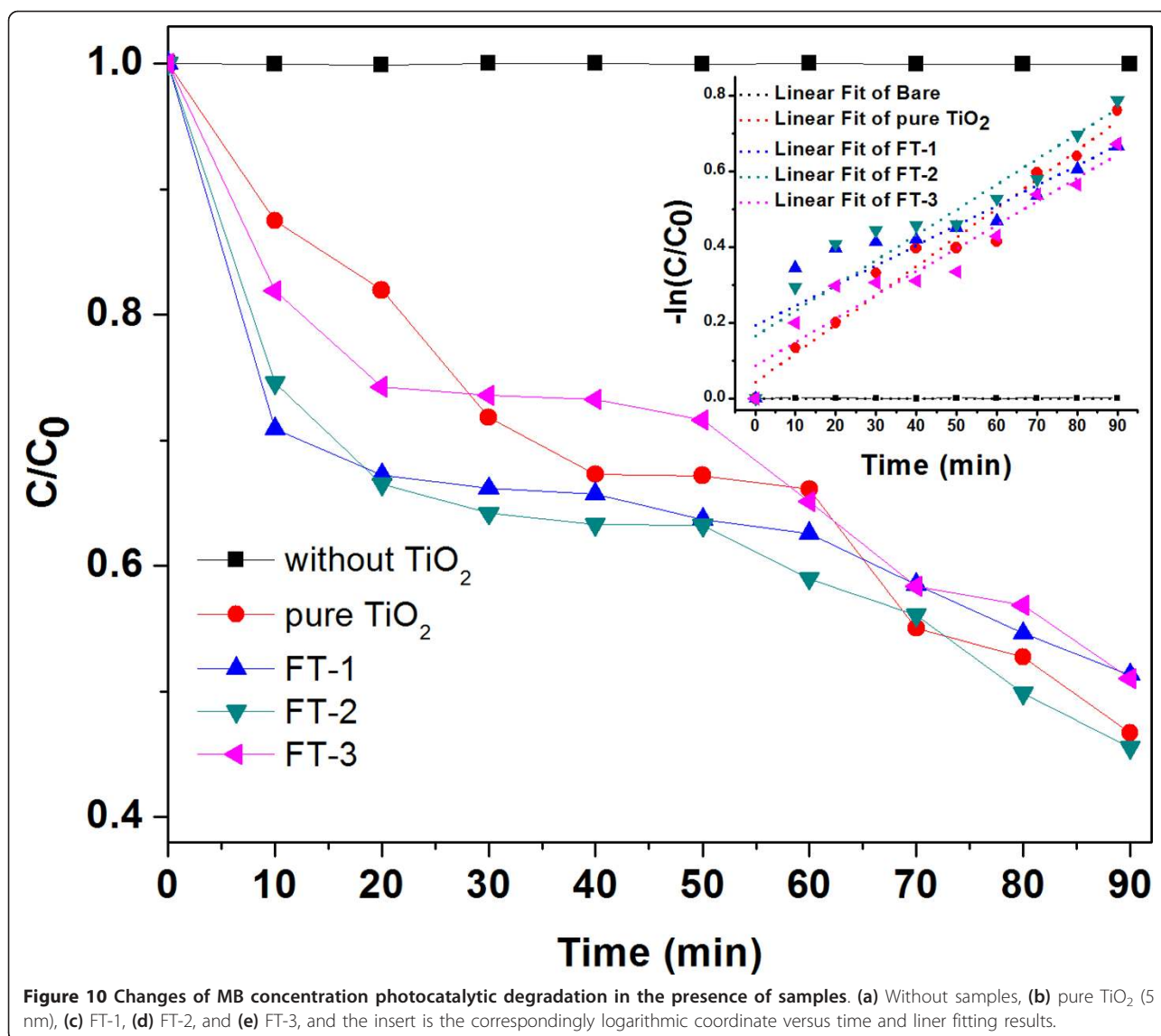| Samples | Chemical composition (%); in parentheses, binding energy (eV) | | | | | Atomic ratio | |
	Ti 2*p*	Fe 2*p*	O 1*s*	N 1*s*	Si 2*p*	Ti/Fe	O/FeTi
FT-1	2.87 (457.7)	1.38 (709.2)	29.08 (529.4)	3.96 (400.3)	3.80 (101.5)	2.08	6.84
FT-2	4.72 (457.8)	1.25 (709.3)	27.13 (529.5)	4.10 (401.2)	2.60 (101.0)	3.78	4.54
FT-3	5.75 (458.3)	1.02 (710.0)	33.53 (530.0)	4.38 (400.7)	5.48 (101.4)	5.63	4.95
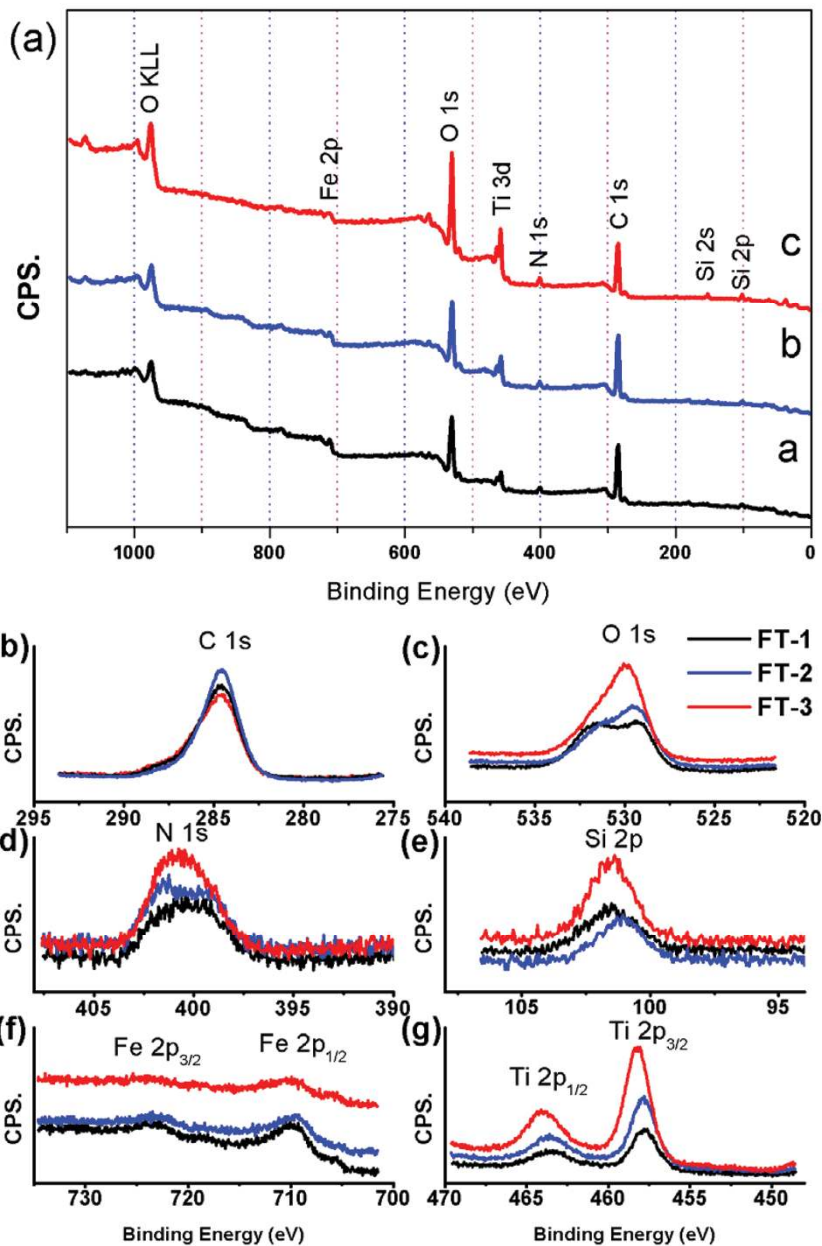
Figure 7 Magnetization vs. filed dependence curves of iron oxides and hybrid NPs. Recorded at T = 300 K. Insert shows the M-H curve of FT-1 samples.
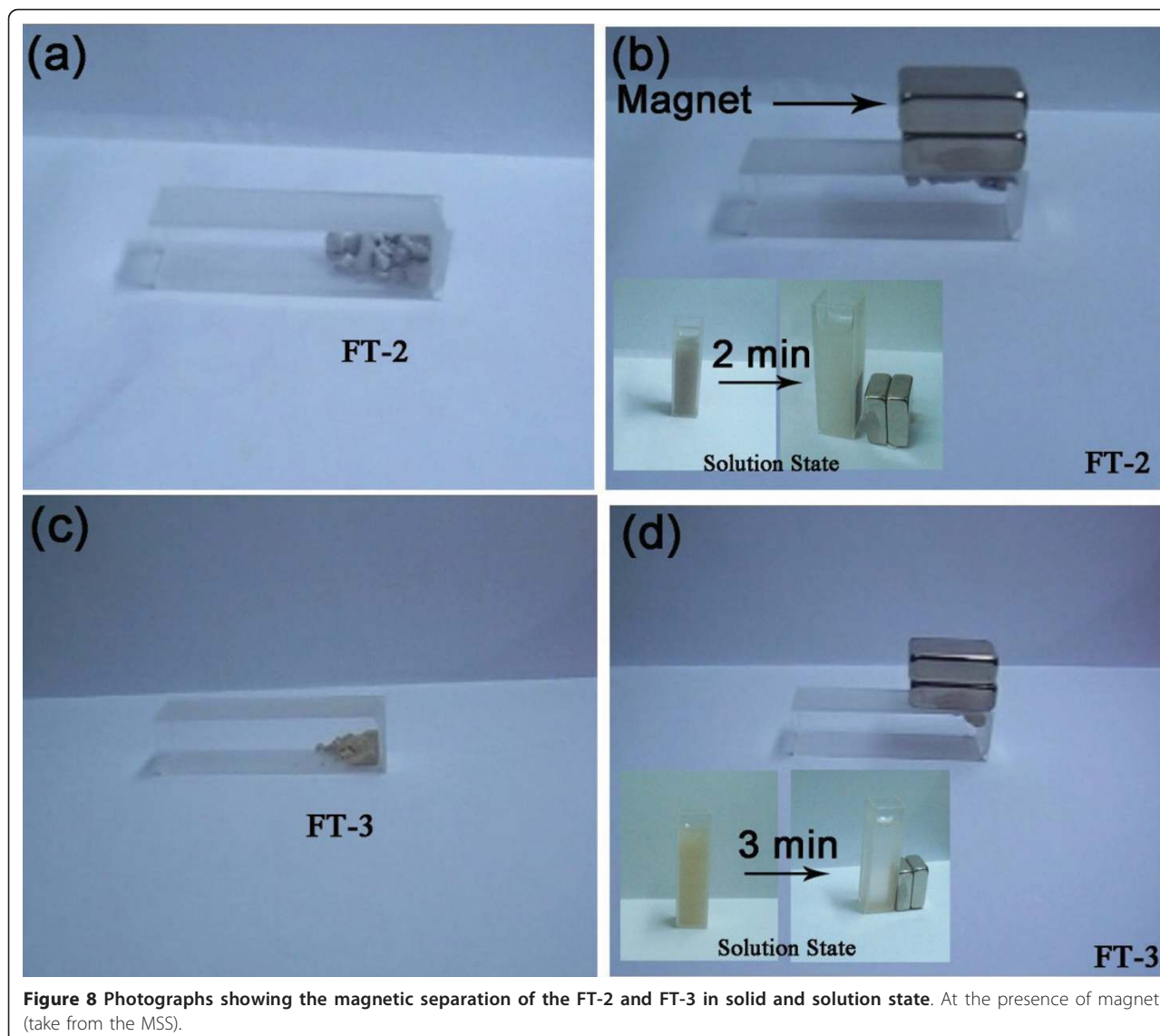
Figure 8 Photographs showing the magnetic separation of the FT-2 and FT-3 in solid and solution state. At the presence of magnet (take from the MSS).
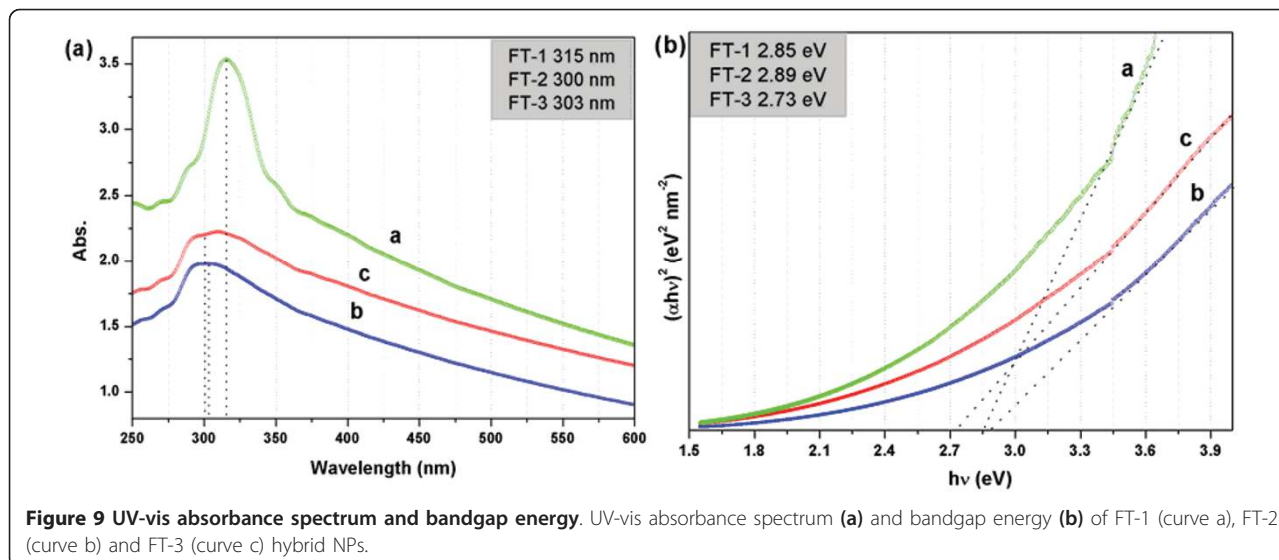
Figure 9 UV-vis absorbance spectrum and bandgap energy. UV-vis absorbance spectrum **(a)** and bandgap energy **(b)** of FT-1 (curve a), FT-2 (curve b) and FT-3 (curve c) hybrid NPs.

Figure 10 Changes of MB concentration photocatalytic degradation in the presence of samples. (a) Without samples, (b) pure TiO_2 (5 nm), (c) FT-1, (d) FT-2, and (e) FT-3, and the insert is the correspondingly logarithmic coordinate versus time and liner fitting results.

of reactant, C is the concentration of reactant, k is the apparent reaction rate constant. The k for FT-1, FT-2, and FT-3 was 1.066% min^{-1}, 1.331% min^{-1}, 1.054% min^{-1}, respectively. It was surprising that the FT-2 exhibited such higher activity. This may be explained by light absorption capability of the FT-2 due to their rough shell contributes to the good photocatalytic activity. Compared to smooth surface, the rough surface layers can absorb more light because the UV-vis light can have multiple-reflections among the shagginess surface structure [74].

Conclusions

In summary, MRCs have been fabricated via a facile seed-mediate technology. These iron oxide/TiO_2 hybrid NPs were synthesized in a stepwise process. First, three different shapes of naked iron oxide NPs were prepared. Next, amino groups encapsulated iron oxide NPs are synthesized by APTES modification. Finally, the iron oxide/TiO_2 hybrid NPs can be obtained after the TiO_2 coating. The FT-2 and FT-3 hybrid NPs show superparamagnetic and both display good photocatalytic properties. This MRCs combination of the photocatalysis properties of TiO_2 and the superparamagnetic property of Fe_3O_4 NPs endows this material with a bright perspective in purification of polluted wastewater. Additionally, this work also discusses the formation mechanism and potentially provided a general method for synthesizing nanocomposites of magnetic iron oxide NPs and other functional NPs, which may find wider applications besides in photocatalysis.

Author details
[1]Key Laboratory of Artificial Micro- and Nano-structures of Ministry of Education, Wuhan University, Wuhan 430072, People's Republic of China [2]Center for Electron Microscopy and School of Physics and Technology, Wuhan University, Wuhan 430072, People's Republic of China [3]School of Printing and Packaging, Wuhan University, Wuhan 430079, People's Republic of China China

Authors' contributions
WW participated in the materials preparation, data analysis and drafted the manuscript. SZ, XX and RF participated in the sample characterization. CZ participated in its design and coordination. All authors read and approved the final manuscript.

Competing interests
The authors declare that they have no competing interests.

References
1. Tian ZRR, Voigt JA, Liu J, McKenzie B, McDermott MJ, Rodriguez MA, Konishi H, Xu HF: **Complex and oriented ZnO nanostructures.** *Nat Mater* 2003, **2**:821-826.
2. Dobson J: **Magnetic nanoparticles for drug delivery.** *Drug Dev Res* 2006, **67**:55-60.
3. Wu W, He QG, Jiang CZ: **Magnetic iron oxide nanoparticles: synthesis and surface functionalization strategies.** *Nanoscale Res Lett* 2008, **3**:397-415.
4. Shokouhimehr M, Piao YZ, Kim J, Jang YJ, Hyeon T: **A magnetically recyclable nanocomposite catalyst for olefin epoxidation.** *Angew Chem Int Ed* 2007, **46**:7039-7043.
5. Babes L, Denizot B, Tanguy G, Le Jeune JJ, Jallet P: **Synthesis of iron oxide nanoparticles used as MRI contrast agents: a parametric study.** *J Colloid Interface Sci* 1999, **212**:474-482.
6. Yao Y, Huang J, Yang J, McIntyre T, Chen J: **Multimodality based diagnosis and treatment of breast cancer cells by magnetic nanoparticles coated by a gold shell with hyperthermia and radiation therapy.** *Radiother Oncol* 2007, **84**:S78-S78.
7. Qian ZY, Men K, Zeng S, Gou ML, Guo G, Gu YC, Luo F, Zhao X, Wei YQ: **Preparation of magnetic microspheres based on Poly(epsilon-caprolactone)-Poly(ethylene glycol)-Poly(epsilon-caprolactone) copolymers by modified solvent diffusion method.** *J Biomed Nanotechnol* 2010, **6**:287-292.
8. Arkhis A, Elaissari A, Delair T, Verrier B, Mandrand B: **Capture of enveloped viruses using polymer tentacles containing magnetic latex particles.** *J Biomed Nanotechnol* 2010, **6**:28-36.
9. He NY, Liu HN, Li S, Tian L, Liu LS: **A novel single nucleotide polymorphisms detection sensors based on magnetic nanoparticles array and dual-color single base extension.** *J Nanosci Nanotechnol* 2010, **10**:5311-5315.
10. Li ZY, He L, He NY, Shi ZY, Wang H, Li S, Liu HN, Dai YB: **An applied approach in detecting E. coli O157:H7 using immunological method based on chemiluminescence and magnetic nanoparticles.** *Acta Chim Sinica* 2010, **68**:251-256.
11. He NY, Li ZY, He L, Shi ZY, Wang H, Li S, Liu HN, Wang ZF: **Preparation of SiO_2/polymethyl methacrylate/Fe_3O_4 nanoparticles and its application in detecting E. coli O157:H7 using chemiluminescent immunological method.** *J Biomed Nanotechnol* 2009, **5**:505-510.
12. He NY, Tian L, Li S, Liu HN, Wang ZF: **An automated MagStation for high-throughput single nucleotide polymorphism genotyping and the dual-color hybridization.** *J Biomed Nanotechnol* 2009, **5**:511-515.
13. Gupta AK, Gupta M: **Synthesis and surface engineering of iron oxide nanoparticles for biomedical applications.** *Biomaterials* 2005, **26**:3995-4021.
14. Janus M, Tryba B, Kusiak E, Tsumura T, Toyoda M, Inagaki M, Morawski A: **TiO_2 nanoparticles with high photocatalytic activity under visible light.** *Catal Lett* 2009, **128**:36-39.
15. Hou YD, Wang XC, Wu L, Chen XF, Ding ZX, Wang XX, Fu XZ: **N-doped SiO_2/TiO_2 mesoporous nanoparticles with enhanced photocatalytic activity under visible-light irradiation.** *Chemosphere* 2008, **72**:414-421.
16. Wu ZB, Gu ZL, Zhao WR, Wang HQ: **Photocatalytic oxidation of gaseous benzene over nanosized TiO_2 prepared by solvothermal method.** *Chin Sci Bull* 2007, **52**:3061-3067.
17. Wang WJ, Zhang JL, Chen F, He DN, Anpo M: **Preparation and photocatalytic properties of Fe^{3+}-doped Ag@TiO_2 core-shell nanoparticles.** *J Colloid Interface Sci* 2008, **323**:182-186.
18. Kwak ES, Lee W, Park NG, Kim J, Lee H: **Compact inverse-opal electrode using non-aggregated TiO_2 nanoparticles for dye-sensitized solar cells.** *Adv Funct Mater* 2009, **19**:1093-1099.
19. Liu B, Aydil ES: **Growth of oriented single-crystalline rutile TiO_2 nanorods on transparent conducting substrates for dye-sensitized solar sells.** *J Am Chem Soc* 2009, **131**:3985-3990.
20. Zhao D, Peng TY, Lu LL, Cai P, Jiang P, Bian ZQ: **Effect of annealing temperature on the photoelectrochemical properties of dye-sensitized solar cells made with mesoporous TiO_2 nanoparticles.** *J Phys Chem C* 2008, **112**:8486-8494.
21. Baek IC, Vithal M, Chang JA, Yum JH, Nazeeruddin MK, Gratzel M, Chung YC, Seok SI: **Facile preparation of large aspect ratio ellipsoidal anatase TiO_2 nanoparticles and their application to dye-sensitized solar cell.** *Electrochem Commun* 2009, **11**:909-912.
22. Cole-Hamilton DJ: **Homogeneous catalysis-new approaches to catalyst separation, recovery, and recycling.** *Science* 2003, **299**:1702-1706.
23. Wang J, Jing LQ, Xue LP, Qu YC, Fu HG: **Enhanced activity of bismuth-compounded TiO_2 nanoparticles for photocatalytically degrading rhodamine B solution.** *J Hazard Mater* 2008, **160**:208-212.
24. Lopez T, Recillas S, Guevara P, Sotelo J, Alvarez M, Odriozola JA: **Pt/TiO_2 brain biocompatible nanoparticles: GBM treatment using the C6 model in Wistar rats.** *Acta Biomater* 2008, **4**:2037-2044.
25. Lv KL, Zuo HS, Sun J, Deng KJ, Liu SC, Li XF, Wang DY: **(Bi, C and N) codoped TiO_2 nanoparticles.** *J Hazard Mater* 2009, **161**:396-401.
26. Xu JJ, Ao YH, Fu D, Yuan CW: **Synthesis of Gd-doped TiO_2 nanoparticles under mild condition and their photocatalytic activity.** *Colloid Surf A* 2009, **334**:107-111.
27. Yue L, Zhang XM: **Preparation of highly dispersed CeO_2/TiO_2 core-shell nanoparticles.** *Mater Lett* 2008, **62**:3764-3766.
28. Li Y, Wu JS, Qi DW, Xu XQ, Deng CH, Yang PY, Zhang XM: **Novel approach for the synthesis of Fe_3O_4@TiO_2 core-shell microspheres and their application to the highly specific capture of phosphopeptides for MALDI-TOF MS analysis.** *Chem Commun* 2008, , **5**: 564-566.
29. Mou F, Guan J, Xiao Z, Sun Z, Shi W, Fan XA: **Solvent-mediated synthesis of magnetic Fe_2O_3 chestnut-like amorphous-core/γ-phase-shell hierarchical nanostructures with strong As(v) removal capability.** *J Mater Chem* 2011, **21**:5414-5421.
30. Guan JG, Mou FZ, Sun ZG, Shi WD: **Preparation of hollow spheres with controllable interior structures by heterogeneous contraction.** *Chem Commun* 2010, **46**:6605-6607.
31. Guan JG, Tong GX, Xiao ZD, Huang X, Guan Y: **In situ generated gas bubble-assisted modulation of the morphologies, photocatalytic, and magnetic properties of ferric oxide nanostructures synthesized by thermal decomposition of iron nitrate.** *J Nanopart Res* 2010, **12**:3025-3037.
32. Tong G, Guan J, Zhang Q: **Goethite hierarchical nanostructures: Glucose-assisted synthesis, chemical conversion into hematite with excellent photocatalytic properties.** *Mater Chem Phys* 2011, **127**:371-378.
33. Chen CT, Chen YC: **Fe_3O_4/TiO_2 core/shell nanoparticles as affinity probes for the analysis of phosphopeptides using TiO_2 surface-assisted laser desorption/ionization mass spectrometry.** *Anal Chem* 2005, **77**:5912-5919.
34. Chen WJ, Tsai PJ, Chen YC: **Functional Fe_3O_4/TiO_2 core/shell magnetic nanoparticles as photokilling agents for pathogenic bacteria.** *Small* 2008, **4**:485-491.
35. Wang CX, Yin LW, Zhang LY, Kang L, Wang XF, Gao R: **Magnetic (γ-Fe_2O_3@SiO_2)$_n$@TiO_2 functional hybrid nanoparticles with actived photocatalytic ability.** *J Phys Chem C* 2009, **113**:4008-4011.

36. Yoon TJ, Lee W, Oh YS, Lee JK: **Magnetic nanoparticles as a catalyst vehicle for simple and easy recycling.** *New J Chem* 2003, **27**:227-229.

37. Ishikawa T, Matijevic E: **Formation of monodispersed pure and coated spindle-type iron particles.** *Langmuir* 1988, **4**:26-31.

38. Wu W, Xiao XH, Zhang SF, Li H, Zhou XD, Jiang CZ: **One-pot reaction and subsequent annealing to synthesis hollow spherical magnetite and maghemite nanocages.** *Nanoscale Res Lett* 2009, **4**:926-931.

39. Massart R: **Preparation of aqueous magnetic liquids in alkaline and acidic media.** *IEEE Trans Magn* 1981, **17**:1247-1248.

40. Wu W, He Q, Chen H: **Silane bridged surface tailoring on magnetite nanoparticles.** *Bioinformatics and Biomedical Engineering* 2007.

41. Wu W, He QG, Chen H, Tang JX, Nie LB: **Sonochemical synthesis, structure and magnetic properties of air-stable Fe_3O_4/Au nanoparticles.** *Nanotechnology* 2007, **18**:145609.

42. Pearson RG: **Hard and soft acids and bases.** *J Am Chem Soc* 1963, **85**:3533-3539.

43. Gillet JN, Meunier M: **General equation for size nanocharacterization of the core-shell nanoparticles by X-ray photoelectron spectroscopy.** *J Phys Chem B* 2005, **109**:8733-8737.

44. Liu SY, Ma YH, Armes SP: **Direct verification of the core-shell structure of shell cross-linked micelles in the solid state using X-ray photoelectron spectroscopy.** *Langmuir* 2002, **18**:7780-7784.

45. Lu LH, Sun GY, Zhang HJ, Wang HS, Xi SQ, Hu JQ, Tian ZQ, Chen R: **Fabrication of core-shell Au-Pt nanoparticle film and its potential application as catalysis and SERS substrate.** *J Mater Chem* 2004, **14**:1005-1009.

46. Remita H, Etcheberry A, Belloni J: **Dose rate effect on bimetallic gold-palladium cluster structure.** *J Phys Chem B* 2003, **107**:31-36.

47. Toshima N, Yonezawa T, Kushihashi K: **Polymer-protected palladium-platinum bimetallic clusters: preparation, catalytic properties and structural considerations.** *J Chem Soc, Faraday Trans* 1993, **89**:2537-2543.

48. Wagner CD, Riggs WW, Davis LE, Moulder JF, Muilenberg GE: *Handbook of X-ray Photoelectron Spectroscopy* Eden Prairie: Perkin-Elmer Corporation, Physical Electronics Division; 1979.

49. Tung WS, Daoud WA: **New approach toward nanosized ferrous ferric oxide and Fe_3O_4-doped titanium dioxide photocatalysts.** *ACS Appl Mater Interfaces* 2009, **1**:2453-2461.

50. Singh H, Laibinis PE, Hatton TA: **Rigid, superparamagnetic chains of permanently linked beads coated with magnetic nanoparticles. Synthesis and rotational dynamics under applied magnetic fields.** *Langmuir* 2005, **21**:11500-11509.

51. Selvan RK, Augustin CO, Sanjeeviraja C, Prabhakaran D: **Effect of SnO_2 coating on the magnetic properties of nanocrystalline $CuFe_2O_4$.** *Solid State Commun* 2006, **137**:512-516.

52. Xuan SH, Jiang WQ, Gong XL, Hu Y, Chen ZY: **Magnetically separable Fe_3O_4/TiO_2 hollow spheres: Fabrication and photocatalytic activity.** *J Phys Chem C* 2009, **113**:553-558.

53. He QH, Zhang ZX, Xiong JW, Xiong YY, Xiao H: **A novel biomaterial - Fe_3O_4:TiO_2 core-shell nanoparticle with magnetic performance and high visible-light photocatalytic activity.** *Opt Mater* 2008, **31**:380-384.

54. Bodker F, Hansen MF, Koch CB, Lefmann K, Morup S: **Magnetic properties of hematite nanoparticles.** *Phys Rev B* 2000, **61**:6826-6838.

55. Mansilla MV, Zysler R, Fiorani D, Suber L: **Annealing effects on magnetic properties of acicular hematite nanoparticles.** *Physica B-Condensed Matter* 2002, **320**:206-209.

56. Tadic M, Kusigerski V, Markovic D, Milosevic I, Spasojevic V: **High concentration of hematite nanoparticles in a silica matrix: structural and magnetic properties.** *J Magn Magn Mater* 2009, **321**:12-16.

57. More AM, Gujar TP, Gunjakar JL, Lokhande CD, Joo OS: **Growth of TiO_2 nanorods by chemical bath deposition method.** *Appl Surf Sci* 2008, **255**:2682-2687.

58. Park JT, Koh JH, Koh JK, Kim JH: **Surface-initiated atom transfer radical polymerization from TiO_2 nanoparticles.** *Appl Surf Sci* 2009, **255**:3739-3744.

59. Segets D, Gradl J, Taylor RK, Vassilev V, Peukert W: **Analysis of optical absorbance spectra for the determination of ZnO nanoparticle size distribution, solubility, and surface energy.** *Acs Nano* 2009, **3**:1703-1710.

60. Sciancalepore C, Cassano T, Curri ML, Mecerreyes D, Valentini A, Agostiano A, Tommasi R, Striccoli M: **TiO_2 nanorods/PMMA copolymer-based nanocomposites: highly homogeneous linear and nonlinear optical material.** *Nanotechnology* 2008, **19**:205705.

61. Pankove JI: *Optical Processes in Semiconductors* Mineola, New York: Courier Dover Publications; 1975.

62. Wu W, Xiao XH, Peng TC, Jiang CZ: **Controllable Ssynthesis and optical properties of connected zinc oxide nanoparticles.** *Chem-Asian J* 2010, **5**:315-321.

63. Fujishima A, Honda K: **Electrochemical photolysis of water at a semiconductor electrode.** *Nature* 1972, **238**:37-38.

64. Chen X, Mao SS: **Titanium dioxide nanomaterials: Synthesis, properties, modifications, and applications.** *Chem Rev* 2007, **107**:2891-2959.

65. Song HM, Ko JM, Park JH: **Hybrid photoreactive magnet obtained from Fe_3O_4/TiO_2 composite nanoparticles.** *Chem Lett* 2009, **38**:612-613.

66. Sato T, Yamamoto Y, Fujishiro Y, Uchida S: **Intercalation of iron oxide in layered $H_2Ti_4O_9$ and $H_4Nb_6O_{17}$: visible-light induced photocatalytic properties.** *J Chem Soc, Faraday Trans* 1996, **92**:5089-5092.

67. Kang M, Choung SJ, Park JY: **Photocatalytic performance of nanometer-sized Fe_xO_y/TiO_2 particle synthesized by hydrothermal method.** *Catal Today* 2003, **87**:87-97.

68. Thongsuwan W, Kumpika T, Singjai P: **Photocatalytic property of colloidal TiO_2 nanoparticles prepared by sparking process.** *Curr Appl Phys* 2008, **8**:563-568.

69. Wu BC, Yuan RS, Fu XZ: **Structural characterization and photocatalytic activity of hollow binary ZrO_2/TiO_2 oxide fibers.** *J Solid State Chem* 2009, **182**:560-565.

70. Xiao Q, Si Z, Zhang J, Xiao C, Zhiming Y, Qiu G: **Effects of samarium dopant on photocatalytic activity of TiO_2 nanocrystallite for methylene blue degradation.** *J Mater Sci* 2007, **42**:9194-9199.

71. Wu W, Xiao X, Zhang S, Zhou J, Ren F, Jiang C: **Controllable synthesis of TiO_2 submicrospheres with smooth or rough surface.** *Chem Lett* 2010, **39**:684-685.

72. Hoffmann MR, Martin ST, Choi W, Bahnemann DW: **Environmental applications of semiconductor photocatalysis.** *Chem Rev* 1995, **95**:69-96.

73. Zhang XW, Du AJ, Lee PF, Sun DD, Leckie JO: **TiO_2 nanowire membrane for concurrent filtration and photocatalytic oxidation of humic acid in water.** *J Membr Sci* 2008, **313**:44-51.

74. Zhang XW, Pan JH, Du AJ, Xu SP, Sun DD: **Room-temperature fabrication of anatase TiO_2 submicrospheres with nanothornlike shell for photocatalytic degradation of methylene blue.** *J Photochem Photobio A* 2009, **204**:154-160.